C-Band SAR Observations of Marginal Ice Zone Rheology in the Labrador Sea

MARK R. DRINKWATER AND VERNON A. SQUIRE

(*Invited Paper*)

***Abstract*—Synthetic Aperture Radar (SAR) imagery collected during the LIMEX'87 field program in the Labrador Sea is used to qualitatively interpret the deformational modes in play throughout the experiment. The ice cover exhibited two distinct rheologies separated by a clear line of shear: A nonlinear viscous outer regime, and a quasi-brittle inner regime. A single constitutive relation capable of effectively modeling both is unlikely within a plastic rate-independent formulation. Rate-dependent effects are discussed in relation to favoring brittle fracture in an otherwise ductile material.**

I. INTRODUCTION

FEW studies of sea ice have employed Synthetic Aperture Radar (SAR) imagery directly for a geophysical purpose. This is undoubtedly due to the complexity and detail of SAR data and the necessity of understanding the scattering of electromagnetic waves by various ice types before the extraction of geophysical parameters can be contemplated. The exception is the abundance of work to determine sea-ice displacement [1]–[5], which demonstrates the potential of SAR in mapping sea-ice motion and deformation fields to a precision, resolution, and spatial coverage that no other technique can match. The drawbacks are that a) these methods presently require a stable satellite orbit, and b) there is a danger of aliasing ice motion in particularly dynamic situations if the satellite repeat is inadequate. Nonetheless, the generation of high-precision sea-ice kinematic data using satellite SAR is one of the most exciting developments in sea-ice research of this decade.

Here we ask the question: Can useful kinematical information be extracted from aircraft SAR data, and further, can the data be used to provide any indications about mesoscale ice rheology? Data used were acquired by the Canada Centre for Remote Sensing (CCRS) 5.3-GHz aircraft SAR system [6] during the March 1987 Labrador Ice Margin Experiment (LIMEX'87). The SAR system achieved a range and azimuth ground resolution of 6 m across an 18-km wide swath, and images were acquired on several flights over the Labrador Sea Marginal Ice Zone (MIZ) in the study region shown in Fig. 1 [7], [8].

Manuscript received December 15, 1988; revised February 20, 1989. This work was partially supported by a National Research Council Resident Research Associateship while under contract to NASA, and by the University of Otago and the University Grants Committee of New Zealand.

M. R. Drinkwater is with the Jet Propulsion Laboratory, California Institute of Technology, 4800 Oak Grove Drive, Pasadena, CA 91109.

V. A. Squire is with the Department of Mathematics and Statistics, University of Otago, P.O. Box 56, Dunedin, New Zealand.

IEEE Log Number 8928692.

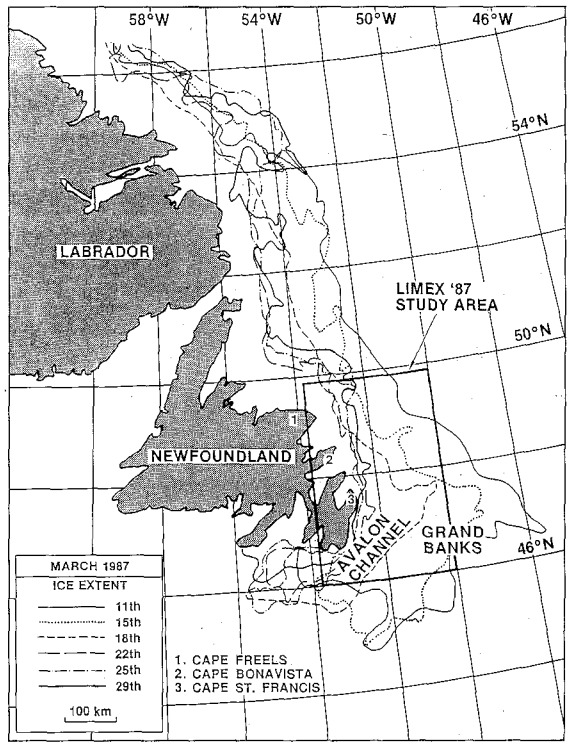

Fig. 1. Labrador Sea marginal ice zone extent during March 1987 and the location of LIMEX'87 operations.

LIMEX'87 afforded the first opportunity to evaluate *C*-band digital SAR data over sea ice in the Grand Banks region off Newfoundland and provides an important preview for ERS-1 and Radarsat satellite data [7].

Local ice floe kinematics and hence ice deformation cannot be derived from the imagery in the sense that [4] derive their results, as aircraft positioning is inadequate without accurate fixed-reference points. Nonetheless, some progress can be made when information on the material that is being imaged, i.e., a nonlinear, ice-water continuum with specific rheological properties, is taken into account. In this way, a single SAR image can provide a qualitative picture of ice rheology, because as a two-dimensional continuum the ice field can only deform, yield, or fracture in well-defined and well-documented ways [9], [10]. At 6 m the resolution of the CCRS SAR is sufficient to study many features in the sea-ice field that can help to suggest a rheological scenario; the presence of a shear zone, for example, can immediately dismiss a simple linearly viscous model.

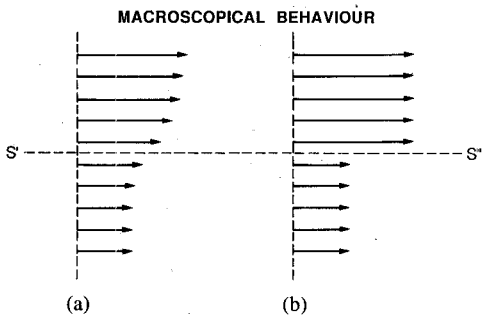

Fig. 2. Displacement in laminar shear flow. (a) Continuous. (b) Discontinuous.

At low strain rates and scales large compared with the characteristic dimensions of the "granular" structure of pack ice, the slow deformational response of the MIZ may be adequately described by plastic shear flow. This type of flow is conceptualized as a single set of infinitesimally close laminae sliding parallel to a shear line (Fig. 2(a)), or alternatively, it may be inhomogeneous and display distinct discontinuities in the displacement along shear lines (Fig. 2(b)). It is fully developed in the sense that continued shear flow leads to large relative displacements between parallel laminae. Plastic shear flow of granular materials is met both in engineering with the flow of bulk materials, and in nature with tectonic faulting or analogous sliding of consolidated materials such as marginal ice. In fully developed shear flow, deformation does not occur until the stress reaches a critical yield level, and it begins and ends without appreciable delay as the stress is first applied and then reduced to subcritical value. Essentially all mechanical energy expended during the flow is dissipated, and when fluidity ceases no mechanical energy is recovered. The SAR imagery reveals several zones within the Labrador Sea MIZ which display some of these characteristics; these are investigated from a rheological standpoint.

Ice rheology is a basic ingredient in dynamical models of sea-ice behavior at all scales. An increased database is required to enable evaluation and reformulation of current models [11] and, when combined with *in situ* data, SAR promises to contribute valuable information for their adaption to marginal ice zones. The discrimination of modes of plastic deformation and the determination of strain rates from SAR imagery, for instance, form a hitherto untapped source of qualitative information which, although not necessarily indicating one rheology categorically, may dismiss others. In this paper we discuss the use of SAR for studying dynamic MIZ phenomena. Processes are studied on the time scale of days, for which synoptic images are available to describe the dynamics and rheology of the region. The implications of these observations for the constitutive laws presently employed in large-scale sea-ice models are discussed.

II. Spring 1987 Grand Banks Sea-Ice Conditions

Under normal circumstances, the Grand Banks region is a classical MIZ in which a seasonally varying ice edge separates a diffuse pack from the open ocean. Meteorological and oceanographic influences strongly modulate the daily extent of the sea-ice cover. MIZ morphology varies on all time and spatial scales due to local interactions and forcing by, for example, swell- and storm-generated waves which break up the ice canopy, or winds and currents which cause ridging and over-rafting of floes. The tongue of ice that stretches down the Newfoundland coast and out over the Grand Banks in winter consists largely of moderately undeformed ice less than 1.5-m thick.

The overall southward flux of ice off the east Newfoundland coast is strongly influenced by ice entrainment within the Labrador coastal current, although the current is largely steered around the broad, shallow continental shelf sea region known as the Grand Banks by submarine topography. Residual currents over the Grand Banks are complicated by the bathymetry, and have typical mean velocities of the order of 5 or 6 cm s^{-1} [12]. However, higher current velocities of the order of 20 cm s^{-1} may be concentrated close to the shore in the Avalon channel, where a filament of the Labrador coastal current is topographically constrained [12], [13].

A. Ice Edge Location and Forcing

During the spring the Grand Banks are normally covered by sea ice and are often the location of the southernmost marginal ice in the Labrador Sea. The month of March is the period of maximum extent, and it also signals the annual break-up and retreat of the ice edge northwestwards along the east coast of Canada. Fig. 1 shows the location of the ice edge during LIMEX'87 [8]. Various studies [14], [15] conclude that a strong correlation exists between weather patterns and the onset of the ice break-up in the Labrador Sea region, and suggest that the ice edge retreat is related to the relative displacement of the 700-mb trough over the eastern Canadian Arctic. Under normal circumstances, the pronounced westerly location of the trough in spring leads to strong west-to-east pressure gradients which result in the northward advection of warm air from the south. Rapid ablation and meltback of the ice edge follows. In March 1987, however, a weaker, more easterly trough resulted in east-to-west pressure gradients, and consequently a reduced frequency of warm southerly winds. Carsey *et al.* [16] show a record of six-hourly averaged wind vectors at St. John's, Newfoundland, for March 6–28, 1987. The record suggests that the general shoreward retreat between March 11–25 mapped in Fig. 1 is largely a compaction in response to a predominance of north–northeasterly winds, rather than a meltback by persistent warm southerlies. However, a particularly vigorous ice compaction event took place between March 16–20 throughout a spell of southeasterlies during the east-to-west passage of two low-pressure cells to the south of Newfoundland.

Using a coupled ice-ocean model of a wind-driven coastal flow with a simplified viscous-plastic rheology [17], [18], Ikeda [19] has demonstrated that alongshore winds, with the coast to the right, lead to a coastal current

(a)

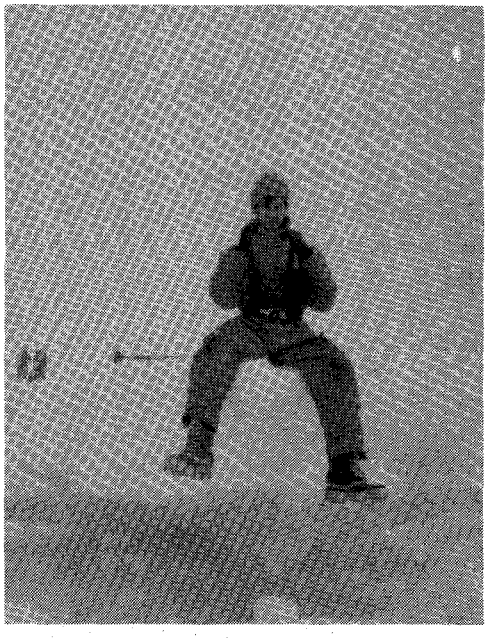

(b)

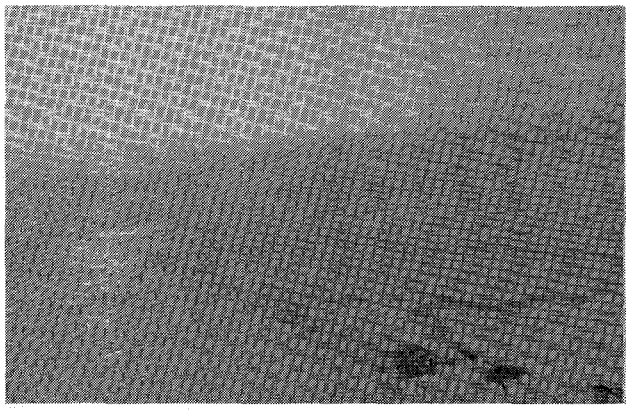

(c)

Fig. 3. Photographs of ice conditions in the marginal ice zone taken by M. Drinkwater during LIMEX'87. (a) Shows a pressure ridge with a sail approximately 2-m in height. (b) Shows a typical rafted block of sea ice, indicating the normal thickness of undeformed first-year ice. (c) Aerial photograph of a typical lead opening along the coastal shear zone.

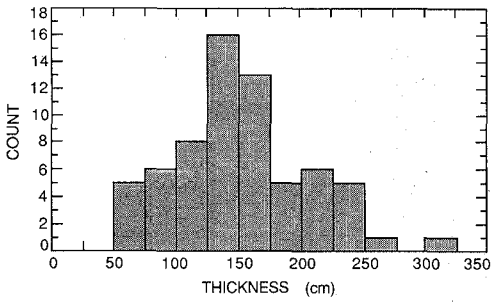

Fig. 4. Ice thickness distribution obtained using measurements taken on March 20, 21, 23, 25, 26, 1987, in the marginal ice from the *CSS Baffin*.

and ice movement, and to a shoreward Ekman flow beneath the ice cover which constrains the Labrador Sea ice over the shelf. When the wind ceases the ice diverges and moves more slowly. The ice velocity is critically sensitive to the shear strength of the sea ice; weak shear strength permits large coastal ice velocities, an intensified Ekman flow, downwelling, and hence a faster coastal current. The alongshore velocity also appears to be affected by onshore winds, which act to increase the shear strength through ice compaction, thereby leading to smaller ice velocities. Offshore winds have the opposite effect.

B. Ice Morphology and Thickness Measurements

The vigorous ice compaction which occurred prior to the acquisition of the SAR images presented in this paper had important consequences for the structure of the ice pack. Ice thickness measurements, and complementary surface and underwater photography (Fig. 3(a)–(c)) collected from the *CSS Baffin* [20] indicate that the high frequency of observations of thick ice near the ice edge was mainly due to the over-rafting of adjacent floes rather than to congelation growth. Sites were selected to be representative of the ice pack near the ship on March 20 and 21, but on March 23, 25, and 26 the measurements were limited by the ice conditions to large cakes in the vicinity. The thickness distribution obtained from all the measurements [20] is shown in Fig. 4. The histogram indicates that the observed mean ice thickness was almost twice the thickness predicted under normal thermodynamic growth (approx. 0.8–1.0 m) [21]. In view of the high incidence of over-rafting observed in underwater photography, the measured thicknesses are probably due to stacked single floes of original thicknesses between 0.5 and 1.24 m. About 30 percent of the ice observed was unrafted, while the proportion of singly and doubly rafted ice was about 50 and 20 percent, respectively. Over half the measurements made were in ice more than 1.5-m thick, with a mean thickness of 1.43 m.

III. SAR Mosaic

Fig. 5 shows a SAR mosaic constructed from data obtained on March 21. The sea ice is compacted into a band of 10/10 concentration along the shoreline. The outer margin of the MIZ is clearly delineated where the radar-bright outer ice zone contrasts with the radar-dark ocean.

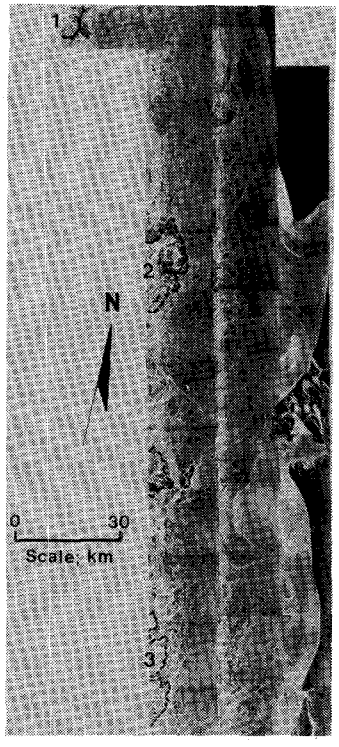

Fig. 5. C-band Synthetic Aperture Radar image mosaic constructed from images taken on March 21, 1987, of pack ice off the Newfoundland coast, by courtesy of CCRS. Numbered coastal locations are: (1) Cape Freels; (2) Cape Bonavista; and (3) Cape St. Francis.

Radar returns from within the pack are not uniform, and a great deal of structure is visible due to variations in surface properties, surface morphology, and floe-size distribution. Examination of the SAR mosaic reveals the two distinct zones [22] which comprise the outer 10–15 km and the inner 20–25 km of the MIZ. The outer zone comprises a slurry of brash and heavily broken-up ice cakes in high concentration, while at the inside edge of this slurry there is an abrupt discontinuity into a different type of ice of altered rheological character. This inner zone is interlaced by a network of intersecting bright lineaments. The main difference between the inner and outer zones is confirmed by ship observations and aerial photography to be the distribution of floe sizes and concentration in each area [22]. The inner zone has a much higher occurrence of large floes with diameters of 17 m or more, with some floe aggregates observed in the 100-m–1-km diameter range. The outer zone is made up of small ice cakes and brash at near 10/10 concentration, forming a slurry continuum of floe sizes from 0 to 20-m across. It is created by flexural breakup and the pommelling of nearby floes through the action of penetrating high-amplitude surface waves. A similar action occurs in the Greenland and Bering Seas [23].

The slurry zone rapidly damps incoming waves, seen propagating into the outer zone of the MIZ from open water in individual SAR scenes [24]; this attenuation is far in excess of the damping associated with sequential scattering by individual ice floes [25]. The incident waves also compact and shear the extreme ice edge [26]. Aggregations of small cakes trapped within the slurry give a bright signature in C-band radar images [22], and serve as passive tracers of the outer zone's response to meteorological or oceanographic forcing.

The transition between the inner and outer zone corresponds to the limit of penetration of high-energy surface gravity waves. Within the interior zone the incoming long waves can bend and fracture the ice, but have insufficient energy to pommel the ice into slurry. In this zone, fractures and nonhomologous ice features provide a deformation time series dating back to several days before the images were collected.

Visual observations of deformed, rafted, and fractured zones of sea-ice floes, which coincide with bright rectilinear features in the radar images, were made from the *CSS Baffin* (see Fig. 3). The 5.6-cm wavelength radar responds with large variations in the backscatter generated by rubble-piled rough ice surfaces or bands of smaller floes generated by grinding or crushing along floe edges. The bright lineaments in Fig. 5 relate to dislocation lines or zones of shear, and also distinguish areas of compressive ridging and rafting or velocity characteristics in the ice field [27]. It is evident from Fig. 5 that the inner zone of the MIZ has a series of dominant regularly spaced fractures running in a northeast–southwest direction. These bright features are criss-crossed by apparently less dominant conjugate fractures yielding acute intersection angles ranging from 30° to 50°, similar to the patterns observed in [9], [10].

IV. MIZ Kinematics From Image Pairs

A. Data Description

SAR images acquired between March 17 and 26 enable a kinematical study of the ice motion to be carried out using image "pairs" with spatially correlated features separated in time. The locations of images used in this analysis are indicated in Fig. 6(a). Spatial overlap was achieved in the Cape Freels coastal region, south Bonavista Bay, and the northern and Cape St. Francis (the northernmost tip of the Avalon peninsula) areas of Conception Bay, permitting coverage of both the inner and outer MIZ.

B. Motion Analysis

Ice motion was derived manually by plotting trajectories of recognizable features for the duration of available overlapping images. Velocity vectors are calculated from their displacement relative to coastal fixed-reference points. In most cases, recognizable features included distinctive ice floe shapes or tonal patterns. Fig. 6(b) illustrates the gross pattern of ice motion vectors and velocities derived from motion pairs spanning the period bracketed by the images.

Detailed analysis of floe velocities reveals a velocity gradient with distance from the shore. More significant, however, is the marked increase in velocities observed at the boundary between the interior ice and the outer slurry

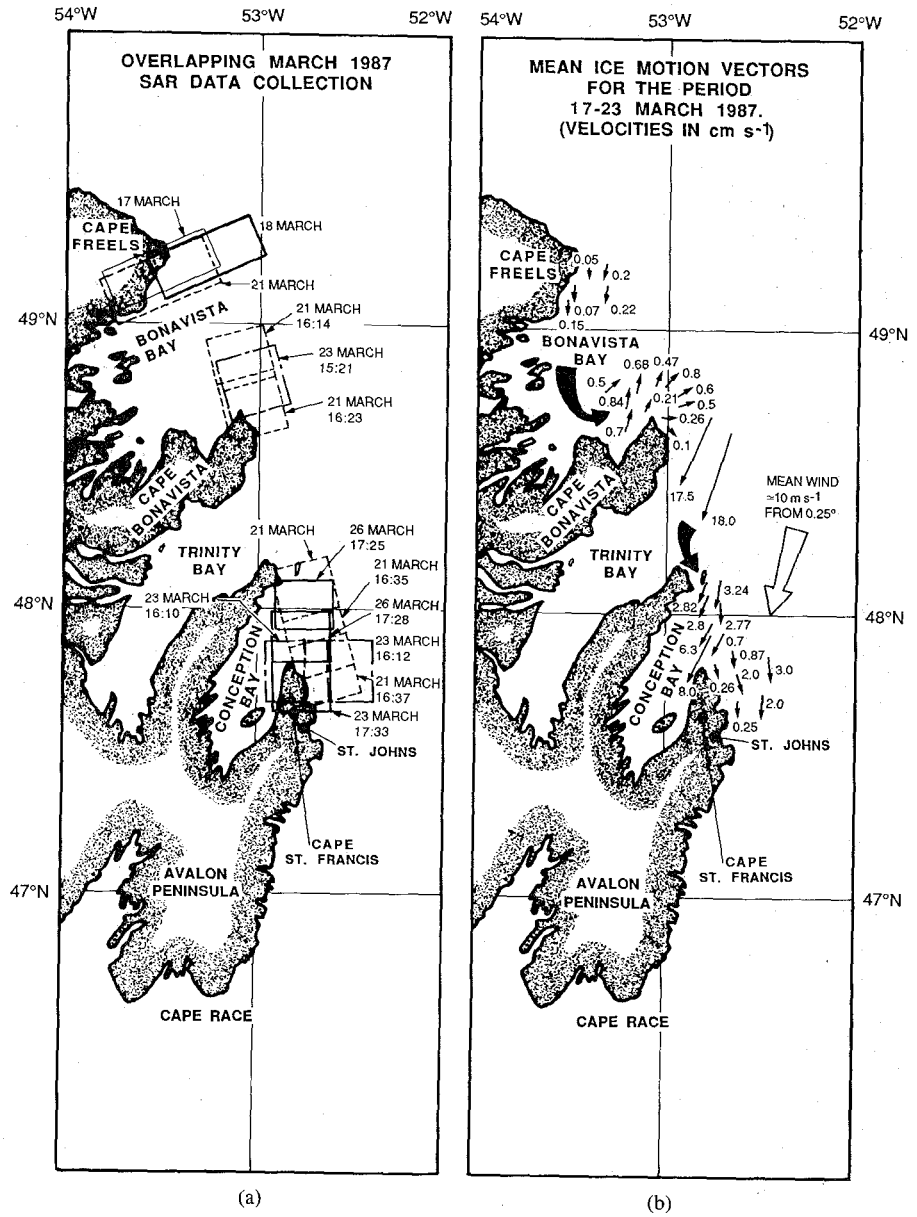

Fig. 6. SAR data used for kinematic analysis: (a) Locations of overlapping images taken at different time intervals. (b) Ice motion field derived from the SAR images.

of wave-pomelled marginal ice. This transitional region within the MIZ is identified as a major line of shear within the pack [21] (cf. Fig. 2). To the east of the line, ice floes travel far more rapidly, at rates more commonly associated with northern sea ice moving along the edge of the Labrador shelf. Speeds of up to 18 cm s^{-1} are seen off Cape Bonavista; comparable with observations of ice motion along the Newfoundland shelf obtained with floe-mounted beacons [28]. Such large velocities are typical of those previously observed in Greenland Sea ice edge jets [29]. Importantly, the north-to-south shear transition becomes better defined between March 21 and 23, when winds shifted from being predominantly southeasterly to north–northeasterly, thereby relieving ice pressure. Ultimately, the advancing front of sea and swell penetration enabled the fracturing of the ice field into smaller floe elements, and by March 26 the bright sinuous features corresponding to areas of dislocation and shear had begun to disappear.

The principal direction of ice advection in the more mobile outer MIZ is generally toward the south, in response to the forcing by the Avalon channel filament of the Labrador current. Mean current speeds in this region are calculated from drift data collected during 1985–1987 to be between 7 and 10 cm s^{-1} [28]. This is in agreement with the current meter measurements made in the same region during LIMEX'87 [30]. Being topographically constrained, the southerly flow of the current in the near-shore region off the northern Grand Banks becomes directed south–southwesterly past St. John's before turning southwestwards around Cape Race at the southern tip of the Avalon peninsula [31].

In some near-shore areas, there is a suggestion of topographic steering of currents or circulatory motions in some anomalous ice-floe trajectories. For example, ice appears to enter Bonavista Bay around Cape Freels, and to leave around Cape Bonavista following the 200-m isobath (Fig. 6(b)). The inflow of ice appears to be occurring around Cape Freels in the north, the ice flowing cyclonically around the Bay and then exiting northeastwards around the northern tip of Cape Bonavista. This observation, although consistent with buoy trajectories [28], is inconsistent with the increased ice pressure induced by the overall westward wind-induced retreat of the ice edge and the general southerly flux of ice. In the shelf region, the dominant tidal constituent has an amplitude of 2–10 cm s^{-1} [32], which may influence ice motion on short time scales. Ice motion trends at longer time scales appear to be closely linked to the prevailing wind direction and influence of the Labrador current.

V. Ice Rheology

To date, most of our ideas on the rheological aspects of ice dynamics and basin-scale sea-ice models have been based on *in situ*, small-scale observations of sea-ice structure and physical properties, taken together with the visual interpretation of surface expressions of deformation such as pressure ridging, over-rafting, or the presence of a shear zone. Moreover, rheological details pertaining to the MIZ have only recently been addressed [11], [18], [33]–[35]. The use of SAR to infer deformational behavior in seasonal pack regions is a promising new alternative to previous methods. *C*-band SAR images acquired during LIMEX'87 are ideal to investigate these ideas because of their remarkable 6-m resolution and because the Labrador Sea, Grand Banks MIZ is varied and dynamic. We begin with a brief review of the deformation of solids.

A. Introduction

Fig. 7 shows the characteristic rheological responses of many materials. As long as we are thinking in terms of *true* stress and *true* strain [36], the curves in Fig. 7(a) are applicable to both tension and compression. The initial linear behavior of the stress σ with strain ϵ in the figure corresponds to elastic deformation. At point A, the yield stress, the elastic limit is reached and the material begins to yield. Beyond A the material undergoes permanent damage and cannot return to its original configuration; it has deformed plastically and is said to be ductile. In the ductile region from point A to point B the plotted curve illustrates strain hardening, a property typical of many materials whereby the material strengthens with the application of the stress so that increased stress is required to increase the strain. This is in contrast to perfect plasticity, where AB would be a line parallel to the strain (ϵ) axis. At point B on the curve, a sample in tension in the laboratory would begin to neck; i.e., the area reduction in some region of the sample would not be compensated by the added strengthening effect of the plastic deformation. Soon after reaching point B the material fails.

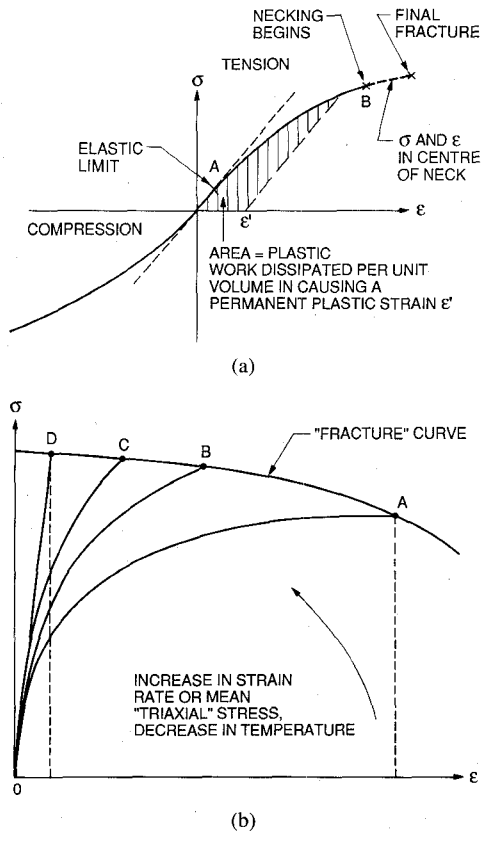

Fig. 7. (a) True stress σ versus true strain ϵ indicating the elastic, plastic, and failure states. A is the yield stress which marks the onset of strain hardening; at B, the material begins to neck (after reference [36]). (b) Family of stress-strain curves showing the influence of factors that tend to promote the brittle fracture of a normally ductile solid (after reference [37]).

Not all materials initially deform elastically; i.e., with an instantaneous and fully recoverable strain, followed by fully irreversible plastic deformation beyond some yield stress, both being independent of time. In many materials, a one–one correspondence between stress and strain no longer prevails and the behavior is time dependent. Such materials are viscoelastic, although it is important to appreciate that we are not limiting the response to linear behavior and that the elastic or viscous contribution may dominate depending upon the level and rate of stress. With a suitable choice of constitutive law, it is possible to include plastic flow within a viscoelastic framework, as will be discussed. Laboratory observations indicate that a general constitutive relation for time-dependent viscoelastic materials should account for the following: Creep (increasing strain at constant stress or load); recovery (decreasing strain when the stress or load is reduced or removed); relaxation (under an induced constant strain the material's stress state decreases with time); and rate effects whereby an increase in the stress or strain rate causes the stress–strain curve to rise more steeply.

The ductile region of a material can be affected by strain rate. As a general rule, the onset of brittle fracture is encouraged by factors which tend to raise the stress–strain curve. This is shown in Fig. 7(b), reproduced from [37].

In this figure, a bounding fracture curve is drawn to intersect the various stress–strain curves representing tensile experiments done at lower temperatures, higher strain rates, or increased "triaxial" stress states (in the *ABCD* direction). The total energy to fracture (i.e., the area beneath the curve) for a material undergoing deformation at high-strain rates, for example, will be much less than that for the same material deforming at low-strain rates. High-strain rates therefore favor a brittle rather than a ductile response.

B. The Labrador MIZ

The well-fractured sea ice of the Labrador MIZ during Spring 1987 was a granular aggregate of various floe sizes and thicknesses. From a physical standpoint, the ice field is a continuum which deforms under the action of forces that induce movements and irrecoverable changes in the relative positions of different parts of itself. The deformation or flow is controlled by the rheology of the continuum, and this is expressed mathematically as a constitutive equation relating the stress and strain rate. A number of isotropic constitutive equations representing rate-independent viscous-plastic ice deformation have been proposed; these are generalized by an expression of the form [16]:

$$\sigma_{ij} = 2\eta d_{ij} + \left[(\zeta - \eta)d_{kk} - P^*/2\right]\delta_{ij} \qquad (1)$$

where σ_{ij} and d_{ij} are the two-dimensional stress and strain rate tensors, respectively, and δ_{ij} is the Kronecker delta. In the most general form of (1) the shear viscosity η, the bulk viscosity ζ, and the ice strength P^* vary spatially and are functions of the strain-rate invariants d_{kk} and d_{ij} d_{ij}. The constitutive equation is a two-dimensional Reiner–Rivlin fluid, which with appropriate simplification will model a variety of rheological behaviors; e.g., Newtonian viscous fluid, viscous-plastic fluid, etc. With varying degrees of success these simplifications have been used to model the dynamics of the entire Arctic and Antarctic sea-ice masses.

There are compelling indications that any reduction of (1) to a linear form will not suffice at these spatial and temporal scales, and that a fully nonlinear constitutive relation is necessary if large-scale features observed in the sea-ice cover are to be adequately modeled. A simple linear Newtonian fluid with no bulk viscosity, for example, will not resist convergence. The inclusion of bulk viscosity to provide compressive strength overcomes this deficiency, but requires different viscosities near to and far from the shore. Nonlinear plastic theories avoid these problems and have been especially successful in modeling the ice of the Arctic Basin. An ice cover has low tensile but high compressive strength; a plastic constitutive law allows this to be implemented simply through the specification of the yield curve. The material's behavior before yield, and the precise form of the yield curve and hence the forms of η, ζ, and P^*, are subjects of debate. Various methods have been used to account for strain hardening (or softening) by making P^* a function of ice thickness and compactness [11], [38]–[40]. These enable the yield surface to grow or shrink isotropically, depending on ice conditions [27]. None, however, have employed kinematic hardening, where the yield curve remains the same size and shape but translates in the normal direction in stress space [41].

C. Balance of Forces

It is possible to estimate the balance of forces acting upon ice floes in the MIZ for two periods of time over which wind and wave measurements were taken [42], as conditions were frequently stationary for periods of more than 12 h. Estimates of air–ice and ice–water stresses are based upon the measured drag coefficients of ice with similar properties to Labrador Sea ice. During the period prior to the acquisition of the mosaic in Fig. 5, winds were predominantly from the southeast (120°) at approximately 6 m s^{-1}, the primary wave system originated from 032° with a significant waveheight of 2.7 m, and the mean current velocity was between 0 and 10 cm s^{-1} [30]. Using these values, mean estimates of wind stress and water stress have been calculated for the period of March 19–21. An ice-wind drag coefficient over rough deformed ice of $C_d = 4.0 \times 10^{-3}$ is assumed after [43]. The value of wind stress is estimated as being approximately $\tau_a = 0.19$ N m^{-2}, while the current stress of $\tau_w = 0.05$ N m^{-2} is based upon typical measured values with currents of this magnitude under similar wind conditions [42].

If the forces upon a floe are assumed to be in equilibrium, then the wind and current stresses when added to the Coriolis force F_c should be balanced by the residual equilibriant; i.e., the internal ice stress F_{int}. On such short time scales, pressure gradient forces generated by the tilt of the ocean are assumed to be unimportant and so are ignored in the balance. Thus, for ice floes far enough into the MIZ to be unaffected by wave radiation stresses, the balance in Fig. 8(a) is assumed for the period of March 19–21. The velocity of the ice is also included, although it does not enter into the balance of forces. Another force balance is constructed for the period of March 21–23, after winds shifted to be predominantly north–northeasterly. The mean wind velocity increased to approximately 10 m s^{-1} from 025°, while the primary wave direction remained at 032° with a significant waveheight of 2.3 m. The balance for this period is shown in Fig. 8(b) for an ice floe in a similar location.

The apparent pattern of stresses for the period of March 21–23 changed significantly with the shift in wind direction on March 21, and the internal ice stress responded accordingly. Prior to March 21, the low wind speed and rapidly decreasing extent meant that winds were not strong enough to significantly change the direction of the motion of the ice. Ice velocity vectors closely followed the predominant current direction, implying that the fetch over the ice was insufficient to generate stresses of sufficient magnitude to overcome the internal ice strength. Between March 21 and 23 the conditions changed, with winds shifting to 025° and increasing to 10 m s^{-1}. The force

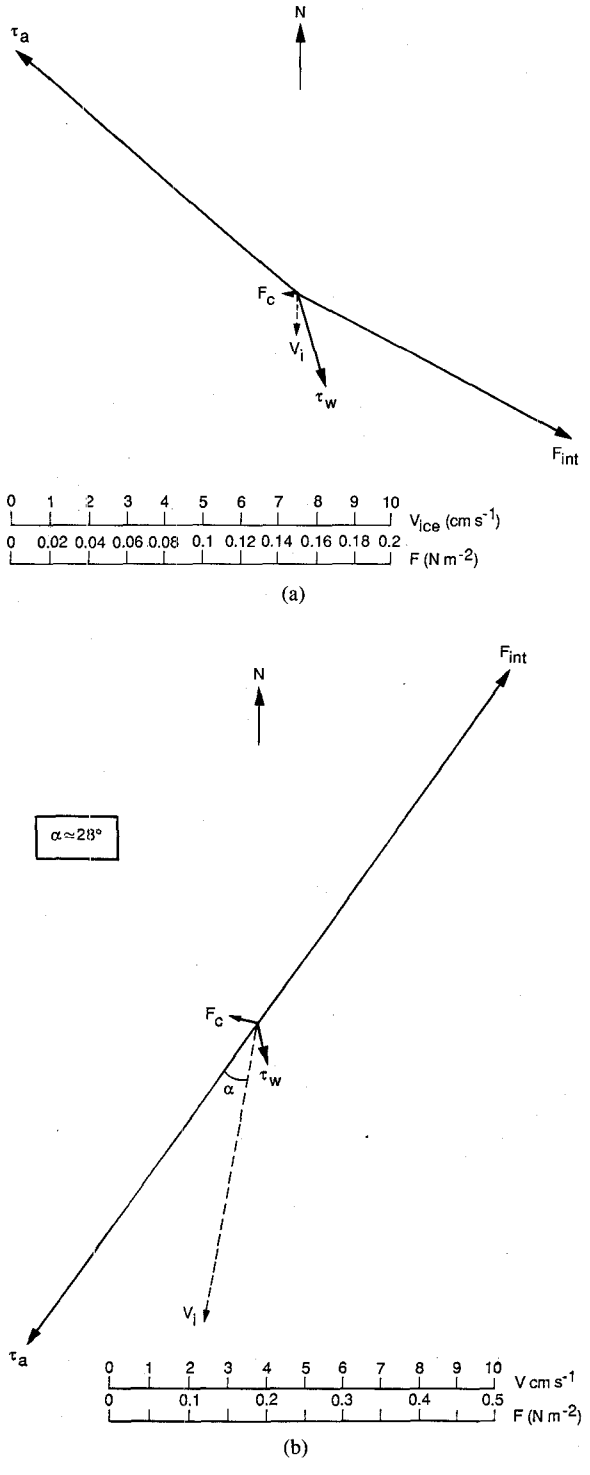

Fig. 8. Balance of forces on ice during two three-day periods in March 1987, and the corresponding deformational response of the ice floe field. (a) Balance of forces under southeasterly winds between March 18 and 21 for ice off the tip of Cape St. Francis. (b) Force balance after winds shifted to north–northeasterlies between March 21 and 23.

balance changed, with a 90° rotation in the orientation of principal stresses to a northeast–southwest direction. Ice-floe trajectories off the northern tip of Cape St. Francis, for example, closely match this direction, and values of V_i increased there to an observed maximum in the inner zone of approximately 8 cm s^{-1}. Importantly, this change in the combination of wind- and current-induced stress appears to be related to the initiation of brittle shear fracture in the ice canopy, since there appears to be little or no permanent deformation preceding it. Ice velocities vectors then traced-out shear lines, becoming rotated through an angle of 10° from their previous direction under the influence of a greater wind stress.

The major effect of southeasterly winds is to rapidly advect outer floes into a more compact MIZ, thereby increasing the packing density of the ice. The only shear lines indicative of principal stress in the northwest–southeast direction are in the Bonavista Bay area, these being consistent with the greater fetches of 80 km or more. Thus, other than in areas with significant fetch, winds appeared to merely precondition the ice field for a subsequent period of rapid shearing which occurred between March 21 and 23. Other major shear lines present in Fig. 5 are indicative of the principal stresses prior to LIMEX'87, and are again consistent with predominantly north–northeasterlies.

D. Observed Rheological Regimes

Preliminary investigation of the image mosaic and velocity fields derived from individual scenes indicates that the deformation of the Labrador Sea MIZ is highly dependent upon geographical location, due to variations in the ice–water mixture making-up the ice canopy, as well as the obvious inhibiting influence of a landmass. Suggestions of both brittle failure and plastic flow are evident in the imagery. The rectilinear shear zones apparent in Fig. 5 are analogous to larger scale features identified in the Canada Basin of the Arctic Ocean [9] and the Fram Strait region of the Greenland Sea [10]. This behavior suggests a brittle failure at high strain rates (as this requires the least energy to fracture), leading to the discontinuous deformation of the compacted ice field. At low strain rates, the ice cover may behave as a rigid (actually highly viscous) or elastic medium at low-stress states, or may flow plastically if the stress reaches the value necessary for the material to yield.

Fig. 9 shows a region within the sea ice around the northern tip of the Avalon peninsula at Cape St. Francis. Recognizable floes have been plotted on March 21, 23, and 26 in Fig. 9 (a)–(c) to indicate the internal motions of the pack across a distinct line of shear. The maximum relative motions on each side of the line indicate that the largest shearing motions occur between March 21 and 23, while by March 26 swell had penetrated and motion ceased. Between March 21 and 23 the maximum velocity differential observed across the shear line was approximately 7 cm s^{-1} (or 6 km d^{-1}). The deformation field is represented in Fig. 9 (d) by polygons drawn around the positions of the homologue marker floes labeled *A–D* in Fig. 9 (a)–(c). The gradient of velocities between floes on March 21 and 23 indicates that there is a considerable mean shear strain rate of 1.24 d^{-1} across the shear line in the east–west direction. Most of the deformation occurs in the plane of the shear line; there are few extensional

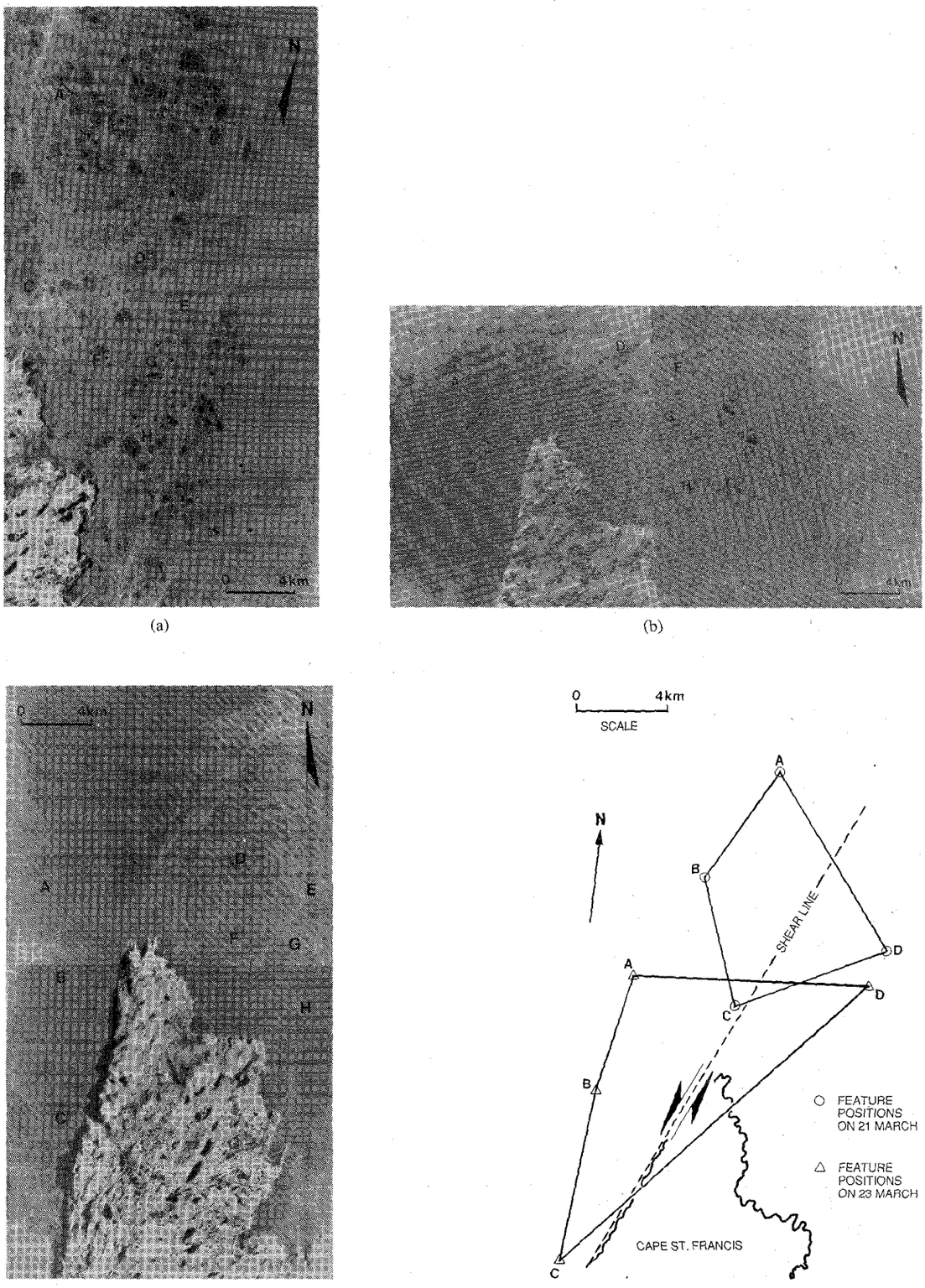

Fig. 9. Series of SAR mosaics constructed from overlapping scenes taken of sea ice off the northern tip of Cape St. Francis on: (a) March 21; (b) March 23; and (c) March 26. Several floes are identified in each image in order to plot ice motion occurring in this region. (d) Deformation polygon showing changes in the relative location of floes labeled *A*, *B*, *C*, *D* for the period March 21–23. Original images were provided by CCRS.

faults, suggesting that tensile stresses did not play a part in the distortion.

The mode of failure illustrated in Fig. 9 (b) and (d) resembles simple shear fracturing. Under biaxial stress, conjugate fracture lines can form, having angles of less than 45° with the direction of maximum compression. As the mobility of the ice improves with an increasing proportion of small floes with distance from the shore, and confining pressure is released, so the relative importance of continuous deformation, as opposed to well-defined lines of fracture, increases. The outer MIZ shows characteristics indicative of the ductile flow, with no recognizable loss in cohesion due to residual ice pressure from wind and wave radiation stresses. Rheologically, the main questions to ask therefore are what conditions lead to the brittle fracture, as opposed to flow, of an ice cover. We need to learn how stress, strain, strain rate, and ice conditions affect ice behavior, and to what degree these conditions are indirectly influenced by local meteorological or oceanographic changes.

The rectilinear shear lines of Figs. 5 and 9(b) may be compared to the strike-slip faults seen in horizontally stressed rock formations. This description of ice was first proposed by Marko and Thomson [9]. Although such features can also be generated by a rate-independent plastic rheology, substantially more work would be required to create the same effect. The association of high strain rates and fracture that was observed during LIMEX'87 therefore conflict with the notion of a rate-independent rheology for the MIZ. Rate-dependent effects are important, as increasing the strain rate encourages brittle fracture at the expense of ductility. The effect of a confining pressure on an ice field is less clear; in rock mechanics, increased pressure leads to greater ductility with less likelihood of fracture. This would seem to be a reasonable hypothesis for the basin-scale modeling of the central Arctic Ocean where ridging and rafting remove energy, but we are unsure of the effect in the MIZ where strain rates are more extreme and the "granular" nature of the material might produce several stages as the ice canopy compresses. Using as an analogy the compression of particulate materials, one might see the ice cover first behaving as though it has a hard structure, then as a particulate, and then at a very high confining pressure (after all open water voids have been removed and rafting and ridging has begun) as a ductile material. The strain-rate effect would offset the move to ductility.

Using the assumption that the sea ice can be approximated as a two-dimensional continuum, we can consider the high strain-rate fracture of ice within the inner zone and investigate the brittle shear failure using a generalization of the Mohr–Coulomb theory [45], [10]. In this theory, failure is assumed to occur when the shear stress reaches a critical value, related to the normal stress. Erlingsson [10] expresses this relation as

$$|\tau_f| = f(\sigma_n, A_i) \qquad (2)$$

where τ_f is the shear stress, σ_n is the normal stress, and the A_i represents the state variables such as temperature, density, etc. Expression (2) represents the Mohr envelope, which in the simple Coulomb theory reduces to a linear form. The Mohr envelope corresponds to a yield surface in the principal axes space. Pritchard *et al.* [46] provide a Mohr envelope for a possible yield surface for sea ice, which allows no tensile strength, includes a compressive cap to limit compressional strength, and has a segment which corresponds to a combination of shear and ridging. The Mohr envelope is more complicated than the Coulomb linear sector, with only a portion of the Coulomb yield surface in either plane strain or plane stress applicable to the sea-ice canopy. In Fig. 9, it is evident that the direction of the principal stress on March 21 in Fig. 8(b) deviates from the shear direction by an angle of about 28°. This suggests that the occurrence of a shear line in this location is consistent with the principal axis of the force balance in Fig. 8(b), and that the stress and velocity characteristics coincide. It is also consistent with the mechanisms involved in shear failure (where failure occurs along a line or conjugate lines forming an angle of less than 45° with the principal stress). The pattern observed implies a coefficient of internal friction of about 0.7, where the coefficient of internal friction is defined by $-df/d\sigma_n|_{Ai}$, of similar magnitude to that observed for ice under conditions of coastal shear and high internal ice stress [47].

In direct contrast to the inner MIZ, the outer MIZ deforms continuously under conditions more typical of viscous, but not Newtonian, flow. This wave-pommelled slurry has a significantly different floe-size distribution and concentration to the interior [22]. Using this technique, a bulk viscosity can be included to allow the constitutive equation to respond to changes in the ice strength induced by factors such as wind, current, and wave-induced radiation stress at the edge. LIMEX'87 observations suggest that the medium flows under any significant applied deviatoric stress, however small, and will suffer continuous change with time. Fig. 10(a) and (b) clearly indicates the differences between the outer MIZ flow regime and the inner MIZ brittle regime. Bands of ice with bright signature have migrated into the ice slurry from the ice edge, and the effect of an eddy is clearly seen, passively traced by the more ductile outer zone. Ductility in a material is known to be affected by the strain rate [37]. Banding indicates the directions of maximum straining, although in places these have become dislocated when the strain rates have become too large for the slurry to respond in creep and a quasi-brittle fracture has occurred. Dislocations such as these and lines of shear are evidence with which to dismiss any simple Newtonian flow model with stress in direct proportion to the strain rate. The fluidity of the ice slurry is highly related to the proximity of the ice edge, and the mean rate of strain observed perpendicular to the edge is in excess of 0.62 d^{-1}. Streamline bands within the ice indicate that the outermost floes are

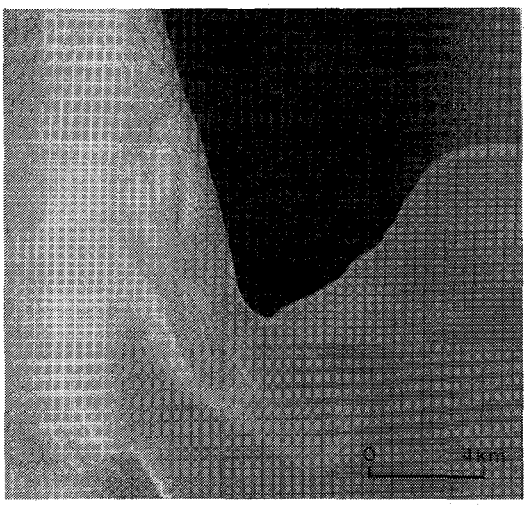

(a)

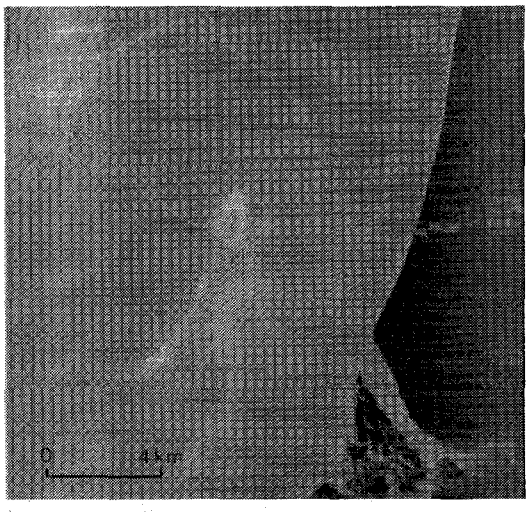

(b)

Fig. 10. Two *C*-band SAR images taken of the outer MIZ on March 21, 1987. (a) Indicates the bright swirls tracing vorticity in the outer edge, some of which have been dislocated by shear activity. (b) Shows a combination of band formation, viscous flow features, and dislocations.

being influenced by both eddy vorticity and an ice-edge jet. In the case of Fig. 10(a), the jet enables the eddy feature to be necked off. The apparent eddy itself is embedded in a field of ice which traces the cyclonic motion, while the southward moving jet continues to export remaining floes in a southward direction.

VI. Discussion

The deformational behavior of sea ice is dependent upon the level of applied stress and upon scale. It is also likely that rate-dependent effects are important in some instances, especially in the premature initiation of brittle fracture. This detail appears to have been largely ignored in the ice modeling literature, where rate-independent plastic rheologies have been adopted. Such rheologies can model dislocations of the kind seen in the LIMEX'87 data [27], but would require more energy to initiate failure. The stress level and strain-rate independence of plastic rheologies can be argued for continuous ice covers, where work goes into building ridges in a rate-independent manner, but this is less clear in the MIZ where strain rates can be much greater. Using the SAR images, strain rates can be calculated directly from the kinematic field in order to look at the relationship and concurrence between high strain rates and fracturing.

It is apparent from the kinematic information derived from Figs. 5, 9, and 10 that two dominant rheological regimes existed during LIMEX'87: An inner zone which exhibited considerable rupture, analogous to discontinuous deformation or brittle fracture in materials of low-fracture toughness; and an outer zone which behaved as a nonlinear viscous fluid. These contrasts in rheology typified the difference between brittle and ductile behavior. The two deformational modes proceeded side-by-side, although the boundary between the two regimes appeared to be determined by the combination of principal stresses and their relative dominance. The shear "line" between the inner and outer zones, for instance, was observed to be either continuous (as on March 21) or discontinuous (as on March 23). This dramatic change occurred as the winds shifted to the east, and as the angle relative to the dominant wave field changed.

It is evident that the conditions experienced during the course of LIMEX'87 were atypical of this locality. The combination of meteorological and oceanographic forces led to rheologies not likely to be experienced under normal, dispersed ice conditions. The LIMEX'87 dataset may therefore be particularly important in untangling the complex problem of MIZ rheology.

SAR can play a major role in investigating the circumstances under which different constitutive relations are realized—the imagery highlights that the Labrador Sea region demonstrates a variety of rheological modes. The LIMEX'87 SAR data have been used to examine the coupling of ice motion with the Labrador Sea current, wind, and wave stresses. Under the conditions experienced in March 1987, the MIZ responded in very different ways, depending upon the combination of stresses and the packing density of the ice. A constitutive relation to effectively describe the rheology of the Labrador Sea MIZ is required for dynamical modeling studies. We still have much work to do, but there are promising developments in the application of granular flow theory to ice-floe rheology, as this provides a theoretical framework for the general analysis of stresses generated by floe collisions [33]. A non-Newtonian rheology of the type described by (1) is found, but with shear and bulk viscosities and a pressure term that depend on the strain rate. The dependence is one-to-one, with stresses depending on the square of the strain rate; the collisional rheology is essentially different from a plastic rheology.

There are several advantages to the use of high-resolution SAR remote-sensing imagery to study sea-ice rheology. Most importantly, time-sequential remotely

sensed images enable the deformation in sea-ice regions to be studied directly and fluxes to be quantified. Such investigations can achieve results concerning the kinematic movements of ice fields and, through associated oceanographic and meteorological data, can quantify the forces that produce the deformations. The use of Synthetic Aperture Radar data, whether provided by satellite or aircraft, will undoubtedly revolutionize our understanding of the dynamics of both marginal and interior sea ice.

Acknowledgment

Especial thanks go to S. Paterson and S. Argus of the Radarsat Project Office at CCRS for supplying the imagery, and to all personnel from the Data Acquisition Division and Airborne Operations Division at the CCRS who contributed to the success of LIMEX'87. Our thanks go also to all other participants of the field experiment who have freely circulated data and allowed this study to be undertaken. We acknowledge the thorough and constructive reviews provided by the reviewers.

References

[1] R. T. Hall and D. A. Rothrock, "Sea ice displacement from SEASAT synthetic aperture radar," *J. Geophys. Res.*, vol. 86, no. C11, pp. 11078–11082, 1978.

[2] F. Leberl, J. Raggam, C. Elachi, and W. J. Campbell, "Sea ice motion measurements from SEASAT SAR images," *J. Geophys. Res.*, vol. 88, no. C3, pp. 1915–1928, 1983.

[3] F. D. Carsey and B. Holt, "Beaufort–Chukchi ice margin data from Seasat: Ice Motion," *J. Geophys. Res.*, vol. 92, no. C7, pp. 7163–7172, 1986.

[4] J. C. Curlander, B. Holt, and K. Hussey, "Determination of sea ice motion from digital SAR imagery," *IEEE J. Oceanic Eng.*, vol. OE-10, no. 4, pp. 358–367, 1985.

[5] M. J. Collins and W. J. Emery, "A computational method for estimating sea ice motion in sequential Seasat synthetic aperture radar imagery by matched filtering," *J. Geophys. Res.*, vol. 93, no. C8, pp. 9241–9251, 1988.

[6] C. E. Livingstone *et al.*, "CCRS *C*-band airborne radar—System description and test results," presented at the 11th Can. Symp. Remote Sensing, Waterloo, Ontario, June 22–25, 1988.

[7] L. McNutt *et al.*, "LIMEX'87: The Labrador Sea Ice Margin Experiment, March 1987," *EOS*, vol. 69, no. 23, p. 634, 1988.

[8] M. R. Drinkwater and S. Digby Argus, "LIMEX'87: An international experiment in the Labrador Sea marginal ice zone," *Polar Rec.*, to be published.

[9] J. R. Marko and R. E. Thomson, "Rectilinear leads and internal motions in the ice pack of the Western Arctic Ocean," *J. Geophys. Res.*, vol. 82, no. 6, pp. 979-987, 1977.

[10] B. Erlingsson, "Two-dimensional deformation patterns in sea ice," *J. Glaciol.*, vol. 34, no. 118, pp. 301–308, 1988.

[11] J. E. Overland and C. H. Pease, "Modeling ice dynamics of coastal seas," *J. Geophys. Res.*, vol. 93, no. C12, pp. 15619-15637, 1988.

[12] D. A. Greenberg and B. D. Petrie, "The mean barotropic circulation on the Newfoundland shelf and slope," *J. Geophys. Res.*, vol. 93, no. 12, pp. 15541–15550, 1988.

[13] B. Petrie and C. Anderson, "Circulation on the Newfoundland Continental Shelf," *Atmos.-Ocean*, vol. 21, no. 2, pp. 207–226, 1983.

[14] R. G. Crane, "Seasonal variations of sea ice extent in the Davis Strait–Labrador Sea area and relationships with synoptic-scale atmospheric circulation," *Arctic*, vol. 31, pp. 434-447, 1978.

[15] R. G. Barry and R. Keen, "Energy budget studies in relation to fast ice breakup processes in Davis Strait, climatological overview," *Institute of Arctic and Alpine Res.*, Univ. of Colorado, Boulder, Occasional Paper No. 26, 1978, pp. 8–67, 1978.

[16] F. D. Carsey *et al.*, "Overview of LIMEX '87 ice observations," *IEEE Trans. Geosci. Remote Sensing*, this issue, pp. 468–482.

[17] W. D. Hibler, "Ice dynamics" in *The Geophysics of Sea Ice*, N. Untersteiner, Ed. New York & London: Plenum, 1986, pp. 577–640.

[18] M. Leppäranta and W. D. Hibler, "The role of plastic ice interaction in marginal ice zone dynamics," *J. Geophys. Res.*, vol. 90, no. C6, pp. 11899–11909, 1985.

[19] M. Ikeda, "A coupled ice-ocean model of a wind-driven coastal flow," *J. Geophys. Res.*, vol. 90, no. C5, pp. 9119–9128, 1985.

[20] B. Holt, *Labrador Ice Margin Experiment—Sea Ice and Remote Sensing Data Report*, RADARSAT Project Office, Ottawa, Ontario, Can., Rep., 1987.

[21] S. Digby Argus, F. D. Carsey, and B. Holt, "Wind, current and swell influences on the ice extent and flux in the Grand Banks–Labrador Sea area as observed in the LIMEX '87 Experiment," in *Proc. 2nd Conf. Polar Meteorol. and Oceanogr.* (Madison, WI), Mar. 29–31, 1988, pp. 11–14.

[22] S. Digby Argus and F. D. Carsey, "SAR imagery of the Grand Banks pack ice and its relationship to surface features" in *Proc. IGARSS'88 Symp.* (Edinburgh, Scotland), 1988.
—— and ——, *ESA SP-284*, vol. 3, pp. 1425–1428, 1988.

[23] V. A. Squire and S. C. Moore, "Direct measurement of the attenuation of ocean waves by pack ice," *Nature*, vol. 283, no. 5745, pp. 365–368, 1980.

[24] P. W. Vachon, R. B. Olsen, C. E. Livingstone, and N. G. Freeman, "Airborne SAR imagery of ocean surface waves obtained during LEWEX: Some initial results," *IEEE Trans. Geosci. Remote Sensing*, vol. 26, no. 5, pp. 548–561, 1988.

[25] P. Wadhams, V. A. Squire, D. J. Goodman, A. M. Cowan, and S. C. Moore, "The attenuation rates of ocean waves in the marginal ice zone," *J. Geophys. Res.*, vol. 93, no. C6, pp. 6799–6818, 1988.

[26] V. A. Squire, "Super-critical reflexion of ocean waves: A new factor in ice edge dynamics?" *Ann. Glaciol.*, to be published.

[27] R. S. Pritchard, "Mathematical characteristics of sea ice dynamics models," *J. Geophys. Res.*, vol. 93, no., C12, pp. 15609–15618, 1988.

[28] I. K. Peterson and G. Symonds, "Ice floe trajectories off Labrador and Eastern Newfoundland: 1985–1987," Bedford Instit. of Oceanogr., Dartmouth, NS, Can. Tech. Rep. of Hydrogr. and Ocean Sci. no. 104, 1988, 101pp.

[29] O. M. Johannessen, J. A. Johannessen, J. Morison, B. I. Farrelly, and E. A. S. Svendsen, "Oceanographic conditions in the zone north of Svalbard in early Fall 1979 with an emphasis on mesoscale processes," *J. Geophys. Res.*, vol. 88, no. C5, pp. 2755–2769, 1983.

[30] C. L. Tang, "Oceanographic observations during LIMEX," Bedford Instit. of Oceanogr., Dartmouth, NS, Can. Data Rep. Hydrogr. and Ocean Sci., no. 72, 1988, 202pp.

[31] J. A. N. Ransom, J. R. Benoit, and F. J. Dello-Stritto, "Ice and ice management on the Grand Bank" in *Proc. Can. East Coast Workshop on Sea Ice*, Jan. 1986, pp. 561–582.

[32] D. B. Fissel and D. D. Lemon, *Analysis of Physical Oceanographic Data from the Labrador Shelf, Summer 1980*, (2 vols.). Sidney, BC: Arctic Sciences, 1982.

[33] H. H. Shen, W. D. Hibler, and M. Leppäranta, "The role of floe collisions in sea ice rheology," *J. Geophys. Res.*, vol. 92, no. C7, pp. 7085–7096, 1987.

[34] M. Ikeda, "A review of sea ice and ocean modeling relevant to the Labrador and Newfoundland shelves," *IEEE Trans. Geosci. Remote Sensing*, this issue, pp. 535–540.

[35] G. M. Flato and W. D. Hibler III, "The effect of ice pressure on marginal ice zone dynamics," *IEEE Trans. Geosci. Remote Sensing*, this issue, pp. 514–521.

[36] M. F. Ashby and D. R. H. Jones, *Engineering Materials: An Introduction to Their Properties and Applications*. New York: Pergamon, 1980, 278pp.

[37] R. M. Caddell, *Deformation and Fracture of Solids*. Englewood Cliffs, NJ: Prentice-Hall, 1980, 307pp.

[38] M. D. Coon, G. A. Maykut, R. S. Pritchard, D. A. Rothrock, and A. S. Thorndike, "Modeling the pack ice as an elastic-plastic material," *Aidjex Bull.*, no. 24, pp. 1–105, 1974.

[39] W. D. Hibler, "Modeling a variable ice thickness sea ice cover," *Mon. Weather Rev.*, vol. 93, no. C12, pp. 1943–1973, 1980.

[40] R. S. Pritchard, "Mechanical behavior of pack ice" in *Mechanics of Structured Media*, part A, A.P.S. Selvadurai, Ed. Amsterdam: Elsevier, pp. 371–405.

[41] L. E. Malvern, *Introduction to the Mechanics of a Continuous Medium*. Englewood Cliffs, NJ: Prentice-Hall, 1969, 713pp.

[42] K. Hunkins, "The oceanic layer and stress beneath a drifting ice floe," *J. Geophys. Res.*, vol. 80, no. 24, pp. 3425–3433, 1975.
[43] P. S. Guest and K. L. Davidson, "The effect of observed ice conditions on the drag coefficient in the summer East Greenland Sea marginal ice zone," *J. Geophys. Res.*, vol. 92, no. C7, pp. 6943–6954, 1987.
[44] D. A. Rothrock, "The mechanical behavior of sea ice" in *Annual Review of Earth and Planetary Sciences*, vol. 3, F. A. Donath, Ed. Palo Alto, CA: Annual Reviews, 1975, pp. 317–342.
[45] G. Ranalli, *Rheology of the Earth: Deformation and Flow Processes in Geophysics and Geodynamics*. Boston: Allen and Unwin, 1987, 366pp.
[46] R. S. Pritchard, R. W. Reimer, and M. D. Coon, 'Ice flow through straits" in *Proc. 5th Int. Conf. on Port and Ocean Eng. under Arctic Conditions (POAC '79)* (Trondheim, Norway), 1979, vol. 3, pp. 61–74.
[47] D. S. Sodhi, "Ice arching and the drift of pack ice through restricted channels," U.S. Army Cold Regions Res. and Eng. Lab., Hanover, NH, CRREL Rep. No. 77-18, 1977, 11pp.

*

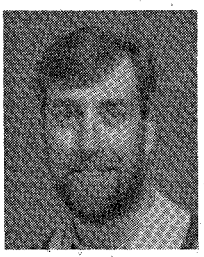

Mark R. Drinkwater received the B.Sc. (Hons.) degree in geography from Durham University (England) in 1984, specializing in remote sensing and glaciology, and the Ph.D. degree in radar remote sensing of polar ice from the Scott Polar Research Institute and Emmanuel College of the University of Cambridge in 1988.

He worked as a Research Scientist for Polar Oceans Associates, a U.K. division of Science Applications, Inc. of San Diego, CA, before joining the Jet Propulsion Laboratory, California Institute of Technology, Pasadena, as a Resident Research Associate. As a Research Associate he has pursued techniques in modeling microwave backscatter properties of snow and ice media. His current research interests as a member of the Polar Oceanography Group include multifrequency polarimetric microwave observations of the marginal ice zone and ice sheets, and in particular the use of Synthetic Aperture Radar for monitoring deformational behavior in sea-ice fields.

Dr. Drinkwater is a member of the International Glaciological Society and the U.K. Remote Sensing Society.

*

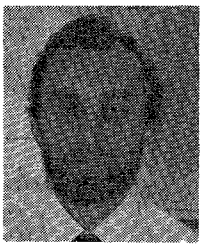

Vernon A. Squire received the B.Sc. (Hons.) degree in applied mathematics from the University College of Wales, Aberystwyth, in 1974. He then joined the Department of Applied Mathematics and Theoretical Physics (DAMTP) and Trinity College at the University of Cambridge to read Part III, specializing in advanced theories of continuum mechanics and fluid dynamics. After graduating from Part III, he moved to another department of Cambridge—the Scott Polar Research Institute—to study for the Ph.D. degree, which was awarded in 1978 for his dissertation entitled *Dynamics of Ocean Waves in a Continuous Sea Ice Cover*.

Before taking up the Chair of Applied Mathematics at the University of Otago, Dunedin, New Zealand, he worked at the University of Cambridge, first as a Research Associate, and later in the established position of Senior Assistant in Research. During this time he took part in some 16 field seasons to the polar regions, and was engaged in related theoretical modeling work in geophysical fluid mechanics, marine engineering, and remote sensing.

Professor Squire was recently awarded the Polar Medal with Arctic and Antarctic Clasp by Her Majesty Queen Elizabeth II for his work during the 16 field seasons to the polar regions. He is a Fellow of the Institute of Mathematics and its Applications, a Fellow of the Royal Geographical Society, and a member of the International Glaciological Society. He is a member of the Ross Dependency Research Committee Physical Sciences Working Group, the International Association for the Physical Sciences of the Ocean Commission on Sea Ice (IAPSO–ICE), the Royal Society of New Zealand National Committee for Theoretical and Applied Mechanics, and other relevant committees.